www.sciencemag.org/content/full/342/6156/341/suppl/DC1

Supplementary Material for

Electron-Hole Diffusion Lengths Exceeding 1 Micrometer in an Organometal Trihalide Perovskite Absorber

Samuel D. Stranks, Giles E. Eperon, Giulia Grancini, Christopher Menelaou, Marcelo J. P. Alcocer, Tomas Leijtens, Laura M. Herz, Annamaria Petrozza, Henry J. Snaith*

*Corresponding author. E-mail: h.snaith1@physics.ox.ac.uk

Published 18 October 2013, *Science* **342**, 341 (2013)
DOI: 10.1126/science.1243982

This PDF file includes:

Materials and Methods

Figs. S1 to S4

Tables S1 to S3

Materials and Methods

Perovskite precursor preparation

Methylamine iodide (MAI) was prepared by reacting methylamine, 33 wt% in ethanol (Sigma-Aldrich), with hydroiodic acid (HI) 57 wt% in water (Sigma-Aldrich), at room temperature. HI was added dropwise while stirring. Upon drying at 100^{o}C, a white powder was formed, which was dried overnight in a vacuum oven and recrystallized from ethanol before use. To form the $CH_3NH_3PbI_{3-x}Cl_x$ or $CH_3NH_3PbI_3$ precursor solution, methylammonium iodide and either lead (II) chloride (Sigma-Aldrich) or lead (II) iodide (Sigma-Aldrich) were dissolved in anhydrous *N*,*N*-Dimethylformamide (DMF) at a 3:1 molar ratio of MAI to $PbCl_2/PbI_2$, with final concentrations 0.88M lead chloride/iodide and 2.64M methylammonium iodide.

Substrate preparation

Glass substrates for absorption, TA and PL measurements were cleaned sequentially in 2% hallmanex detergent, acetone, propan-2-ol and oxygen plasma. Devices were fabricated on fluorine-doped tin oxide (FTO) coated glass (Pilkington, $7\Omega\,\square^{-1}$). Initially FTO was removed from regions under the anode contact, to prevent shunting upon contact with measurement pins, by etching the FTO with 2M HCl and zinc powder. Substrates were then cleaned and plasma-etched as above. A hole-blocking layer of compact TiO_2 was deposited by spin-coating a mildly acidic solution of titanium isopropoxide in ethanol, and annealed at 500°C for 30 minutes. Spin-coating was carried out at 2000rpm for 60 seconds.

Perovskite deposition

To form the perovskite layer for spectroscopy measurements, the non-stoichiometric precursor was spin-coated on the substrate at 2000rpm in air. For $CH_3NH_3PbI_{3-x}Cl_x$, the precursor was used as is; for the $CH_3NH_3PbI_3$, the precursor was diluted in DMF at a 1:1 ratio of precursor to DMF. After spin-coating, the $CH_3NH_3PbI_{3-x}Cl_x$ films were annealed at 100°C for 45 minutes, and the $CH_3NH_3PbI_3$ at 150°C for 15 minutes. The top quenchers were then deposited in air via spin-coating chlorobenzene solutions with the following conditions: poly(methylmethacrylate) (PMMA; Sigma-Aldrich) at 10mg/ml and phenyl-C_{61}-butyric acid methyl ester (PCBM; Solenne BV) at 30mg/ml, both spin-coated at 1000rpm, and 2,2’,7,7’-tetrakis-(N,N-di-p-methoxyphenylamine)9,9’-spirobifluorene (spiro-OMeTAD; Borun Chemicals) at 0.46M spin-coated at 2000rpm.

For devices, the perovskites were prepared by spin-coating in a nitrogen-filled glovebox. The $CH_3NH_3PbI_{3-x}Cl_x$ precursor was used as is and the $CH_3NH_3PbI_3$ was spin-coated from a precursor solution diluted to 3:5 ratio of precursor to DMF. After spin-coating, films were left to dry at room temperature in the glovebox for 30 minutes. The $CH_3NH_3PbI_{3-x}Cl_x$ films were then annealed on a hotplate at 90°C for 2 hours, and the $CH_3NH_3PbI_3$ films at 170°C for 15 minutes. The spiro-OMeTAD hole-transporting layer was then deposited in air from a 0.79M chlorobenzene solution containing additives of lithium bis(trifluoromethanesulfonyl)imide and 4-tert-butylpyridine. Devices were then left overnight in air. Finally, 60nm gold electrodes were thermally evaporated under vacuum of ~10^{-6} Torr, at a rate of ~0.1nm/s, to complete the devices.

Characterization

A field emission scanning electron microscope (Hitachi S-4300) was used to acquire SEM images. Sample thicknesses were measured using a Veeco Dektak 150 surface profilometer.

Steady-state and transient absorption measurements

Steady-state absorption spectra were acquired with a Varian Cary 300 UV/Vis spectrophotometer using an integrating sphere to account for optical losses outside of the active layer. Nanosecond transient absorption measurements were carried out with a LP920 laser flash spectrometer (Edinburgh Instruments). It is based on a standard Transient Absorption setup where the sample is excited by a ns laser pulse and the time evolution of the differential absorption changes induced by the pump is monitored by a cw light source probe. The pump pulses are provided by a nanosecond tunable OPOLett-355II laser (10 Hz repetition rate). The probe light is provided by a pulsed Xenon arc lamp. The sample was kept at a 45° angle to the excitation beam. The beams are focused onto the sample ensuring spatial overlap. The transmitted probe is spectrally filtered by a monochromator and detected. Two different detection systems are used: a cooled ICCD camera which enables us to detect the entire spectral range from 350 to 850 nm at once and a set of photomultipliers (with both VIS and near-IR detection window) enabling one to collect the single-wavelength kinetic with higher sensitivity. The signal is finally recorded by a TDS 3032C digital signal analyzer. From the transmission change following photoexcitation the variation in the absorption is thus derived as

$$\Delta OD(\tau,\lambda) = \log\left(\frac{I_{probe}}{I_t(\tau,\lambda)}\right) \qquad \text{(S1)},$$

where I_{probe} is the transmitted probe with excitation off and I_t is the transmitted probe after laser excitation. The PL, which appears at ~770nm and is shifted relative to the photobleach (~750nm), was removed by subtracting spectra recorded without the probe beam. The system has a sensitivity of $\sim 5\cdot 10^{-4}$ and a temporal resolution of ~ 8 ns. The excitation density was tuned from 4 $\mu J/cm^2$ to 40 $\mu J/cm^2$ but negligible effects on the dynamics were observed on these time scales. The data were fitted with biexponential functions of the form $A_1\exp(-t/\tau_1) + A_2\exp(-t/\tau_2)$, where A_1 and A_2 are prefactors and τ_1 and τ_2 are time constants. The fitted parameters are presented in Table S3. The quoted errors in the biexponential fits arise directly from the fitting procedure.

Photoluminescence measurements and fits

Steady-state and time-resolved PL measurements were acquired using a time-correlated single photon counting (TCSPC) setup (FluoTime 300, PicoQuant GmbH). Film samples were photoexcited using a 507nm laser head (LDH-P-C-510, PicoQuant GmbH) pulsed at frequencies between 0.3-10MHz, with a pulse duration of 117ps and fluence of ~30nJ/cm^2. The samples were exposed to the pulsed light source for ~10-30 minutes prior to measurement to ensure stable sample emission. The PL was collected using a high resolution monochromator and hybrid photomultiplier detector assembly (PMA Hybrid 40, PicoQuant GmbH).

Parameters describing the photoluminescence dynamics in the absence of any quencher are required inputs in the diffusion model. These were obtained by fitting the background-corrected PL measured from PMMA-capped perovskite films with a stretched exponential decay function of the form,

$$I(t) = I_0 e^{-(t/\tau_s)^{\beta_s}} \qquad \text{(S2).}$$

Errors in the fitting parameters were determined by examining the reduced χ^2 surfaces obtained by independently varying each fitting parameter. A cut-off value of $\chi_R^2(p)/\chi_R^2 = 1.2$ was used in each case to obtain limits at a confidence level of 68 %. For ease of comparison of lifetimes between samples with different quenchers, τ_e is defined as the time taken after excitation for the PL intensity to drop to 1/e of its peak intensity. The error in the accuracy of this lifetime was taken to be the half of the range of points whose mean value lies within one standard deviation of the 1/e line. The PL decay parameters are summarised in Table S2.

Diffusion modeling

The PL decay dynamics were modeled by calculating the number and distribution of excitations in the film $n(x,t)$ according to the 1-D diffusion equation,

$$\frac{\partial n(x,t)}{\partial t} = D\frac{\partial^2 n(x,t)}{\partial x^2} - k(t)n(x,t) \qquad \text{(S3),}$$

where D is the diffusion coefficient and $k(t)$ is the PL decay rate in the absence of any quencher material (*22*). The total decay rate, $k = k_f + k_{nr} = \beta\tau_s^{-\beta_s}t^{\beta_s-1}$, was determined by fitting a stretched exponential decay to the PL data measured from perovskite layers with PMMA and assumed independent of the capping material. The effect of the quenching layer was included by assuming that all excitons which reach the interface are quenched with unit efficiency ($n(L,t)=0$, where $x=0$ at the glass/perovskite interface and L is the perovskite film thickness). As the excitation pulse was from the glass substrate side of the samples, the initial distribution of excitons was taken to be $n(x,0)=n_0 exp(-\alpha x)$, where $\alpha=A/L$ (absorbance at 507 nm / perovskite layer thickness). Any deviation from this distribution due to reflection of the laser pulse at the perovskite/quencher interface was assumed to be negligible. In order to calculate the diffusion length L_D, the diffusion coefficient was varied to minimize the reduced chi-squared value,

$$\chi_r^2 = \frac{1}{(n-p-1)}\sum\frac{\left(y(t)-y_c(t)\right)^2}{y(t)} \qquad \text{(S4),}$$

where $y(t)$ and $y_c(t)$ are the measured and calculated PL intensities at time t, n is the number of data points and p is the number of fitting parameters (*27*). The equation was solved numerically using the Crank-Nicholson algorithm and the number of excitons integrated across the entire film in order to determine the total PL intensity at time t. Both the stretched exponential and 1-D diffusion models were fit to the experimental TCSPC data by iterative reconvolution with the instrument response function (IRF) which was recorded separately, such that the observed PL intensity,

$$I(t) = \int g\,(t)f(t-t')dt' \qquad \text{(S5),}$$

is the result of the real decay curve, *f(t)*, convolved with the IRF, *g(t)(27)*. The average diffusion length L_D is given by $L_D = \sqrt{D\tau_e}$, where τ_e is the time taken for the PL to fall to 1/e of its initial intensity in the absence of any quencher. The errors reported in the text account for errors in the fitting procedure and in sample thickness, with the latter providing the most significant contribution. The root-mean-square errors in the thickness were determined to be ±40nm for the mixed halide and ±35nm for the triiodide using a surface profilometer and atomic force microscopy (data not shown).

Solar cell characterization

The current density–voltage (J-V) curves were measured (2400 Series SourceMeter, Keithley Instruments) under simulated AM 1.5 sunlight at 100 mWcm^{-2} irradiance generated by an Abet Class AAB sun 2000 simulator, with the intensity calibrated with an NREL calibrated KG5 filtered Si reference cell. The mismatch factor was calculated to be less than 1%. The solar cells were masked with a metal aperture to define the active area, typically 0.09cm^2 (measured individually for each mask) and measured in a light-tight sample holder to minimize any edge effects and ensure that the reference cell and test cell are located in the same spot under the solar simulator during measurement.

Supplementary Text

Perovskite coverage

Figures S1 and S2 show SEM cross- and top-section images of the mixed halide and triiodide perovskite samples, respectively. The top-view images show that the perovskite coverage is >91% for the mixed halide and >85% for the triiodide as calculated using a method shown elsewhere (*26*). Since the film thicknesses (~180nm and ~270nm) are much smaller than the spacing between the areas without perovskite, the fraction of excitations created near the "pore walls" that will diffuse laterally to the quencher on the pore wall before reaching the top quencher will be negligible. Hence, our diffusion length results are not affected by the incomplete coverage.

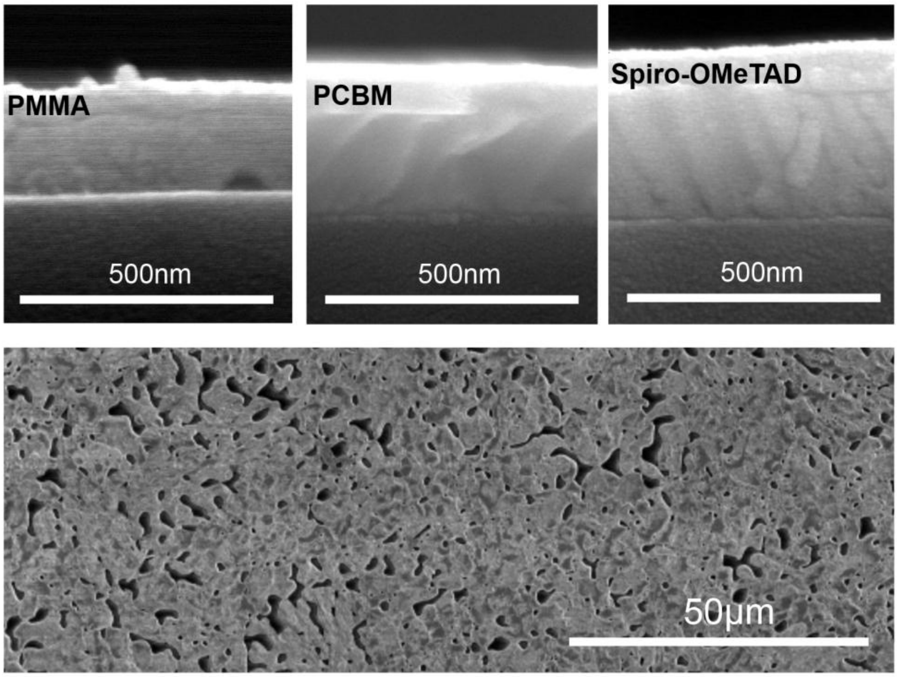

Fig. S1. ***Top*****:** Cross-sectional SEM images of the measured ~270nm $CH_3NH_3PbI_{3-x}Cl_x$ films formed on glass, coated with the quenching/non-quenching layer as labelled. ***Bottom*****:** Top view SEM of the morphology of a pristine $CH_3NH_3PbI_{3-x}Cl_x$ film formed on glass.

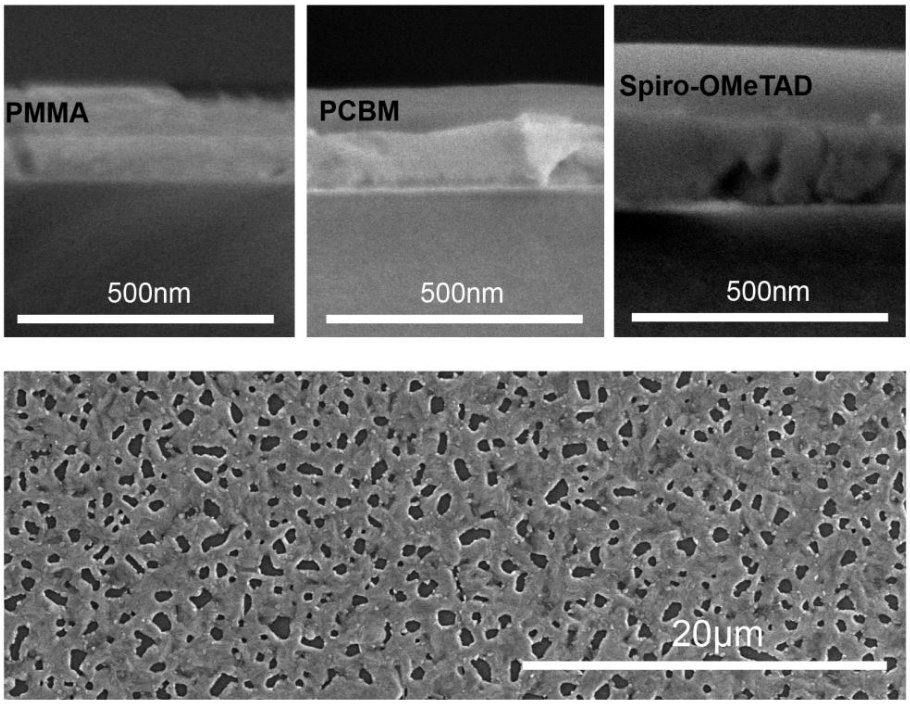

Fig. S2. ***Top*****:** Cross-sectional SEM images of the measured ~180nm $CH_3NH_3PbI_3$films formed on glass, coated with the quenching/non-quenching layer as labelled. ***Bottom*****:** Top view SEM of the morphology of a pristine $CH_3NH_3PbI_3$ film formed on glass.

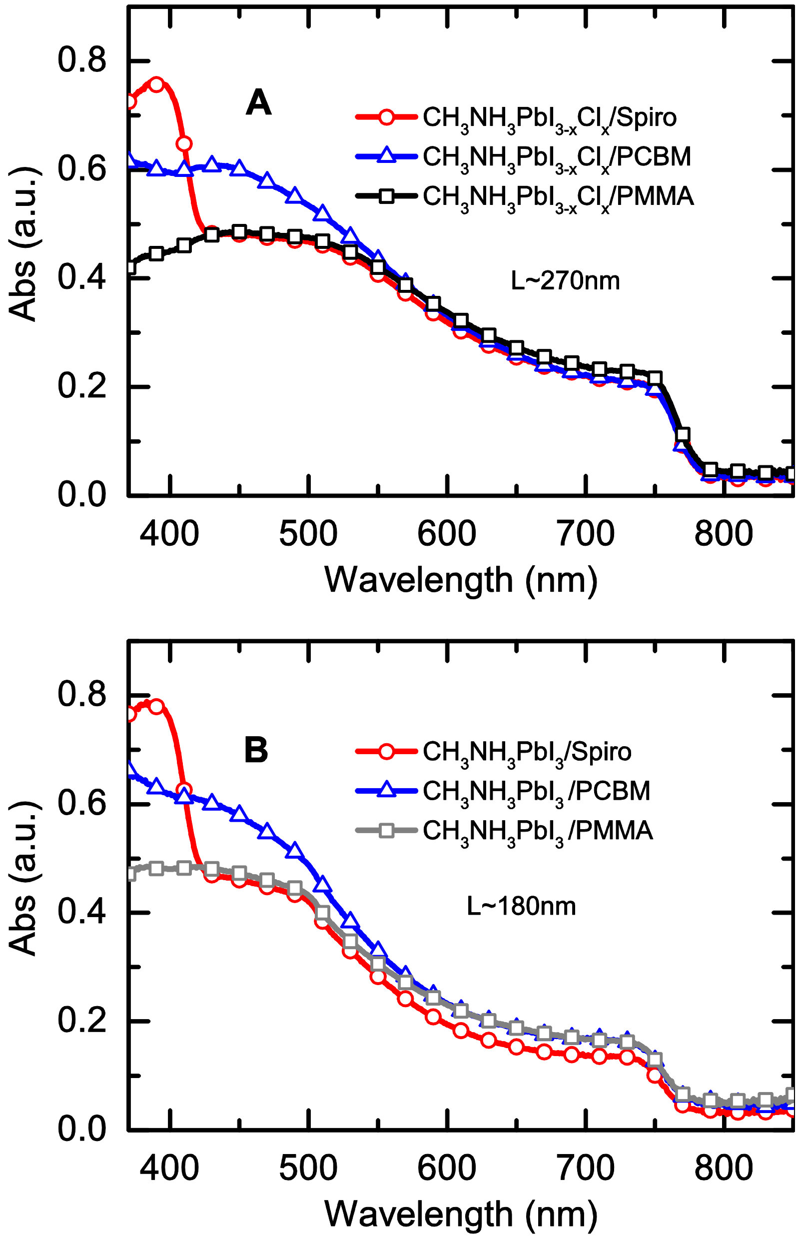

Fig. S3. Absorption spectra of the quenching samples under investigation comprised of the **(A)** mixed halide $CH_3NH_3PbI_{3-x}Cl_x$, and **(B)** triiodide $CH_3NH_3PbI_3$ perovskites. The thicknesses *L* are also shown.

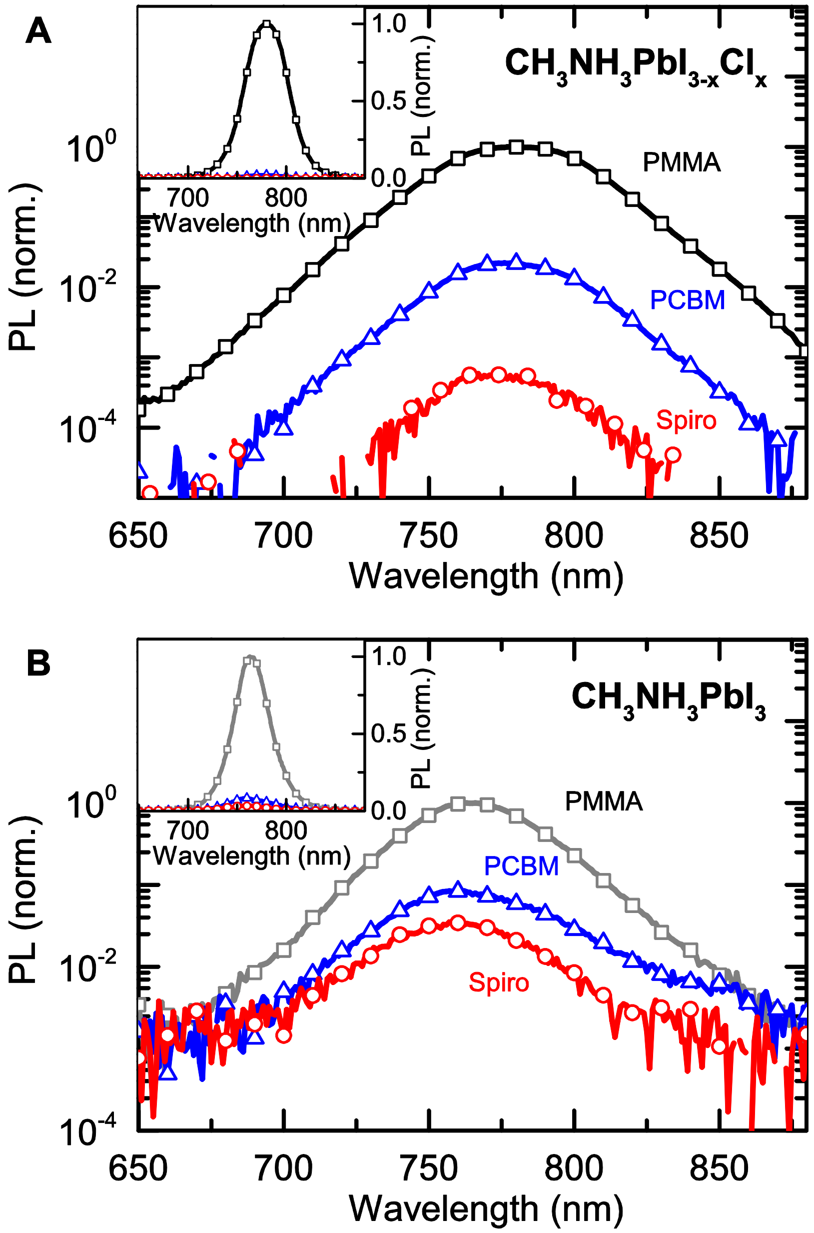

Fig. S4. Steady-state PL spectra of the quenching samples under investigation comprised of the **(A)** mixed halide $CH_3NH_3PbI_{3-x}Cl_x$, and **(B)** triiodide $CH_3NH_3PbI_3$ perovskites. Excitation was at 507nm, and through the glass substrate side. *Insets*: PL presented on linear scales.

Table S1. Table showing average device performance parameters extracted from current-voltage characteristics for a batch of devices fabricated using the optimized protocols for each perovskite. Devices were measured under 100mWcm^{-2} simulated AM1.5G illumination. Errors represent the standard deviation in the batch.

Perovskite	**No. devices**	**J_{sc} (mAcm^{-2})**	**V_{oc} (V)**	**Fill Factor**	**PCE (%)**
$CH_3NH_3PbI_{3-x}Cl_x$	9	13.1±4.3	0.89±0.10	0.59±0.14	7.8±4.0
$CH_3NH_3PbI_3$	8	7.7±3.4	0.72±0.08	0.44±0.09	2.3±1.3

Table S2. Table summarizing the fitting parameters obtained from fits to the photoluminescence data in Figure 2. τ_e is the time taken after excitation for the PL intensity to drop to 1/e of the peak intensity, and τ_s and β_s are parameters obtained from stretched exponential fits to the PMMA data. The parameters and associated errors are discussed in detail in the Materials and Methods section.

Perovskite	**Quencher**	**τ_e (ns)**	**τ_s (ns)**	**β_s**
$CH_3NH_3PbI_{3-x}Cl_x$	PMMA	272.65±6.95	285.7±11.7	0.833±0.032
	PCBM	6.12±0.10	-	-
	Spiro	5.12±0.06	-	-
$CH_3NH_3PbI_3$	PMMA	9.60±0.26	8.00±0.33	0.767±0.025
	PCBM	3.17±0.03	-	-
	Spiro	4.22±0.06	-	-

Table S3. Table summarizing the parameters obtained from fits to the transient absorption data in Figure 1C using functions of the form $A_1\exp(-t/\tau_1) + A_2\exp(-t/\tau_2)$. We note that the photobleach decay curve is presented in Figure 1C as normalized ΔO.D., while the photoabsorption decay remains as ΔO.D.

Feature	**A_1**	**τ_1 (ns)**	**A_2**	**τ_2 (ns)**
Photobleach (750nm)	0.904±0.006	283.0±5.8	0.201±0.007	2337.7±117.3
Photoabsorption (550nm)	0.0074±0.0001	288.0±11.6	0.0049±0.0002	5863.9±698.4

References and Notes

1. S. Chu, A. Majumdar, Opportunities and challenges for a sustainable energy future. *Nature* **488**, 294–303 (2012). doi:10.1038/nature11475 Medline

2. B. O'Regan, M. Gratzel, A low-cost, high-efficiency solar cell based on dye-sensitized colloidal TiO2 films. *Nature* **353**, 737–740 (1991). doi:10.1038/353737a0

3. Z. He, C. Zhong, S. Su, M. Xu, H. Wu, Y. Cao, Enhanced power-conversion efficiency in polymer solar cells using an inverted device structure. *Nat. Photonics* **6**, 593 (2012). doi:10.1038/nphoton.2012.190

4. R. A. J. Janssen, J. Nelson, Factors limiting device efficiency in organic photovoltaics. *Adv. Mater.* **25**, 1847–1858 (2013). doi:10.1002/adma.201202873 Medline

5. T. Todorov, D. B. Mitzi, Direct liquid coating of chalcopyrite light-absorbing layers for photovoltaic devices. *Eur. J. Inorg. Chem.* **2010**, 17–28 (2010). doi:10.1002/ejic.200900837

6. E. H. Sargent, Colloidal quantum dot solar cells. *Nat. Photonics* **6**, 133–135 (2012). doi:10.1038/nphoton.2012.33

7. M. Graetzel, R. A. J. Janssen, D. B. Mitzi, E. H. Sargent, Materials interface engineering for solution-processed photovoltaics. *Nature* **488**, 304–312 (2012). doi:10.1038/nature11476 Medline

8. G. Hodes, D. Cahen, All-solid-state, semiconductor-sensitized nanoporous solar cells. *Acc. Chem. Res.* **45**, 705–713 (2012). doi:10.1021/ar200219h Medline

9. G. Yu, J. Gao, J. C. Hummelen, F. Wudl, A. J. Heeger, Polymer photovoltaic cells: Enhanced efficiencies via a network of internal donor-acceptor heterojunctions. *Science* **270**, 1789–1791 (1995). doi:10.1126/science.270.5243.1789

10. O. V. Mikhnenko, H. Azimi, M. Scharber, M. Morana, P. W. M. Blom, M. A. Loi, Exciton diffusion length in narrow bandgap polymers. *Energy Environ. Sci.* **5**, 6960 (2012). doi:10.1039/c2ee03466b

11. J. J. M. Halls, C. A. Walsh, N. C. Greenham, E. A. Marseglia, R. H. Friend, S. C. Moratti, A. B. Holmes, Efficient photodiodes from interpenetrating polymer networks. *Nature* **376**, 498–500 (1995). doi:10.1038/376498a0

12. M. M. Lee, J. Teuscher, T. Miyasaka, T. N. Murakami, H. J. Snaith, Efficient hybrid solar cells based on meso-superstructured organometal halide perovskites. *Science* **338**, 643–647 (2012). doi:10.1126/science.1228604

13. H.-S. Kim, C. R. Lee, J. H. Im, K. B. Lee, T. Moehl, A. Marchioro, S. J. Moon, R. Humphry-Baker, J. H. Yum, J. E. Moser, M. Grätzel, N. G. Park, Lead iodide perovskite sensitized all-solid-state submicron thin film mesoscopic solar cell with efficiency exceeding 9%. *Sci. Rep.* **2**, 591 (2012). doi:10.1038/srep00591 Medline

14. J. H. Heo, S. H. Im, J. H. Noh, T. N. Mandal, C.-S. Lim, J. A. Chang, Y. H. Lee, H.- Kim, A. Sarkar, M. K. Nazeeruddin, M. Grätzel, S. I. Seok, Efficient inorganic-organic hybrid heterojunction solar cells containing perovskite compound and polymeric hole conductors. *Nat. Photonics* **7**, 486 (2013). doi:10.1038/nphoton.2013.80

15. J. H. Noh, S. H. Im, J. H. Heo, T. N. Mandal, S. I. Seok, Chemical management for colorful, efficient, and stable inorganic-organic hybrid nanostructured solar cells. *Nano Lett.* **13**, 1764–1769 (2013). Medline

16. J. M. Ball, M. M. Lee, A. Hey, H. J. Snaith, Low-temperature processed meso-superstructured to thin-film perovskite solar cells. *Energy Environ. Sci.* **6**, 1739 (2013). doi:10.1039/c3ee40810h

17. J. Burschka, N. Pellet, S. J. Moon, R. Humphry-Baker, P. Gao, M. K. Nazeeruddin, M. Grätzel, Sequential deposition as a route to high-performance perovskite-sensitized solar cells. *Nature* **499**, 316–319 (2013). doi:10.1038/nature12340 Medline

18. A. Abrusci, S. D. Stranks, P. Docampo, H. L. Yip, A. K. Jen, H. J. Snaith, High performance perovskite-polymer hybrid solar cells via electronic coupling with fullerene monolayers. *Nano Lett.* **13**, 3124–3128 (2013). doi:10.1021/nl401044q Medline

19. M. Liu, M. B. Johnston, H. J. Snaith, Efficient planar heterojunction perovskite solar cells by vapour deposition. *Nature* **501**, 395–398 (2013). doi:10.1038/nature12509 Medline

20. W. Zhang, M. Saliba, S. D. Stranks, Y. Sun, X. Shi, U. Wiesner, H. J. Snaith, Enhancement of perovskite-based solar cells employing core-shell metal nanoparticles. *Nano Lett.* **13**, 4505–4510 (2013). doi:10.1021/nl4024287 Medline

21. A. Kojima, K. Teshima, Y. Shirai, T. Miyasaka, Organometal halide perovskites as visible-light sensitizers for photovoltaic cells. *J. Am. Chem. Soc.* **131**, 6050–6051 (2009). doi:10.1021/ja809598r Medline

22. P. E. Shaw, A. Ruseckas, I. D. W. Samuel, Exciton diffusion measurements in poly(3-hexylthiophene). *Adv. Mater.* **20**, 3516–3520 (2008). doi:10.1002/adma.200800982

23. T. Ishihara, Optical properties of PbI-based perovskite structures. *J. Lumin.* **60-61**, 269–274 (1994). doi:10.1016/0022-2313(94)90145-7

24. K. Tanaka, T. Takahashi, T. Ban, T. Kondo, K. Uchida, N. Miura, Comparative study on the excitons in lead-halide-based perovskite-type crystals $CH_3NH_3PbBr_3$ $CH_3NH_3PbI_3$. *Solid State Commun.* **127**, 619–623 (2003). doi:10.1016/S0038-1098(03)00566-0

25. M. Hirasawa, T. Ishihara, T. Goto, K. Uchida, N. Miura, Magnetoabsorption of the lowest exciton in perovskite-type compound $(CH_3NH_3)PbI_3$. *Physica B* **201**, 427–430 (1994). doi:10.1016/0921-4526(94)91130-4

26. G. E. Eperon, V. M. Burlakov, P. Docampo, A. Goriely, H. J. Snaith, Morphological control for high performance, solution-processed planar heterojunction perovskite solar cells. *Advanced Funtional Materials*, published online 9 September 2013 (10.1002/adfm.201302090).

27. J. R. Lakowicz, *Principles of Fluorescence Spectroscopy* (Springer London, Limited, 2007).